Simultaneous Measurements of Photoabsorption and Photoelectrochemical Performance for Thickness Optimization of a Semiconductor Photoelectrode

Naoya Murakami,[1,2,*] *Ryo Watanabe*[1]

[1]Graduate School of Life Science and Systems Engineering, Kyushu Institute of Technology, 2-4 Hibikino, Wakamatsu-ku, Kitakyushu 808-0196, Japan

[2]Department of Applied Chemistry, Faculty of Engineering, Kyushu Institute of Technology, 1-1 Sensuicho, Tobata, Kitakyushu 804-8550, Japan

KEYWORDS

Semiconductor photoelectrode, Photoacoustic, Thickness optimization

ABSTRACT

We established a system for simultaneous measurements of photoelectrochemical (PEC) reaction and photoabsorption in a semiconductor photoelectrode. This system uses a photoacoustic technique and photoelectrodes with a film-thickness gradient that were prepared by electrophoretic

deposition of tungsten(VI) oxide particles while pulling up a substrate. The system enabled high-throughput determination of optimum film thickness, and the results showed that irradiation direction has a significant influence on PEC performance for a photoelectrode with a thick film. Furthermore, the mechanism of enhancement of PEC performance by post-necking treatment was discussed.

INTRODUCTION

Photoelectrochemical (PEC) water splitting over n-type and p-type semiconductor electrodes has been intensively studied because this method can drive up-hill reactions, such as water splitting and carbon dioxide reduction, using inexhaustible solar energy.[1-6] In the case of an n-type semiconductor electrode, excited electrons and positive holes, which are generated as a result of photoabsorption of incident light, induce reduction on the counter electrode and oxidation on the semiconductor surface, respectively. Therefore, film thickness is a fundamental parameter for a photoelectrode because photoabsorption monotonically increases as a function of film thickness, showing a saturation tendency when thickness is close to the penetration depth of photoexcitation. However, performance, so that, Faradaic photocurrent sometimes does not show monotonic increase as film thickness because the photocurrent depends on not only photoabsorption but also recombination rate, which is changed by film thickness.[7,8] Determination of the optimum thickness by PEC measurements of many samples with various thickness is usually time-consuming and costly. Therefore, research and development of a PEC system using a photoelectrode can be accelerated if thickness optimization is achieved by a high-throughput method such as the screen system utilized in optimization of photoelectrode, overcoating and co-catalyst materials.[9-11]

One possible method for high-throughput optimization of thickness is simultaneous measurements of PEC reaction and thickness. Although the thickness of a photoelectrode is frequently measured by cross-sectional observation using a scanning electron microscope, this cannot be applied to simultaneous measurement with PEC reaction. Absorption spectroscopic analysis is one candidate for simultaneous measurements, but conventional transmission spectroscopy cannot be applied to an opaque film. In contrast, the photoacoustic (PA) technique can be applied to simultaneous measurements, regardless of sample transparency. The PA technique is a method for absorption spectroscopy that is applicable to even opaque and strongly scattering materials because it detects photoabsorption indirectly through photothermal waves generated by relaxation of the photoexcited states.[12,13] We have so far set up various in-situ measurement systems including PEC reaction over a photoelectrode[14] and a particulate photocatalyst.[15,16] Here, we propose a simple method for thickness optimization by combination of the PA technique and step scanning of focused laser light. In order to accomplish it, a photoelectrode with a film-thickness gradient was prepared by electrophoretic deposition of tungsten(VI) oxide (WO_3) particles while pulling up the substrate. We examined the correlation between photoabsorption and photocurrent for as-prepared samples with and without post-necking treatment, which is known to enhance PEC performance of a photoelectrode.[17-21]

EXPERIMENTAL

Chemicals and Materials

Iodine, acetone, and sodium sulfate (Na_2SO_4) were purchased from Wako Chemical. WO_3 particles (Aldrich, 550086) and ammonium metatungstate hydrate ($(NH_4)_6H_2W_{12}O_{40}\cdot xH_2O$) were purchased from Sigma-Aldrich.

Preparation of WO_3 Photoanodes

A WO_3 film as an n-type semiconductor was deposited on a fluorine-doped tin oxide-coated (FTO) glass substrate by electrophoretic deposition (EPD).[17-19] Acetone solution (50 mL) containing WO_3 particles (80 mg) and iodine (ca. 10 mg) was irradiated with ultrasound for 30 min. Two parallel 15 mm × 30 mm FTO glass substrates (Geomatec, 10 ohm/sq, 0.5 mmt) were immersed in the solution (5 mL) with a separation of 8 mm, and a bias of 20 V was applied between them. During EPD, a cathode FTO glass was pulled up at a speed of 5.0 mm/min using a z-axis stage (Suruga-Seiki, B05-23K) connected to a stepping motor, which was controlled by a stage controller (Sigma-Koki, SHOT-602). A schematic illustration of EPD for preparation of a photoelectrode with a film-thickness gradient is shown in Figure 1. After EPD, the cathode FTO glass with deposition of WO_3 was heated at 120 ^oC for 5 min. The above process was repeated 4 times, and heat treatment using an electric furnace at 500 °C for 30 min was finally performed. Cross-sectional and top-view images of photoelectrode were observed using field-emission scanning electron microscopy (FE-SEM; JEOL, JSM-6701FONO).

For post-necking treatment of the WO_3 photoelectrode[20,21], the as-prepared electrodes were treated twice with 10 μL of ammonium metatungstate methanol solution (1.0 mmol/L) and then dried in air at room temperature. Finally, samples without and with post-necking treatment were

heated in air at 500 °C for 30 min. The samples prepared without and with post-necking treatment are denoted as wo-PN and w-PN, respectively.

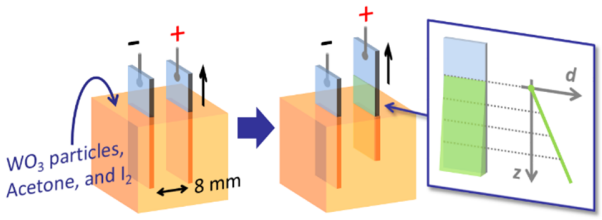

Figure 1. Schematic illustration of EPD for preparation of a photoelectrode with a film-thickness gradient.

Simultaneous PEC and PA measurements

PEC measurement using a three-electrode type cell (Ag/AgCl as a reference electrode and Pt as a counter electrode) and a potentiostat (Princeton Applied Research, 263A) equipped with a lock-in amplifier (Stanford Research Systems, SR830) and PA measurement were carried out simultaneously. The electrolyte used was 0.1 mol/L Na_2SO_4 (pH 6.1). A homemade PA cell with an acrylic body and a quartz window was used. The PA cell was attached to the back side (glass side) of a sample electrode, and photoirradiation was carried out from the glass side or sample side. A laser diode module (Edmund Optics, 37-025, 405 nm) was used as the light source for PEC and PA measurements, and the output intensity was modulated at 2.6 Hz. Vertical step scanning of laser irradiation every 0.02 mm was performed using z-axis stages (Sigma-Koki, TARW-25503L) equipped with a stepping motor, which was controlled by a stage controller (Sigma-Koki, GSC-

01). A schematic illustration of the system for simultaneous PEC and PA measurements is shown in Figure 2. The PA signal was acquired by a digital MEMS microphone (Knowles, SPK0641HT4H-1) buried in the cell and recorded using a PC equipped with a digital I/O interface. Time-series data were acquired by Fourier transformation of the PA signal with a Hamming window function. The obtained data were modified in order to perform correction of the irradiation direction and position. From the PEC measurements at 960 mV vs reversible hydrogen electrode (RHE) of applied potential, which was converted from 400 mV vs Ag/AgCl, incident photon-to-current conversion efficiency (IPCE) was calculated from the photocurrent (j_{ph}) measured using the following equation:

$$\text{IPCE}\ (\%) = 100 \times (1240 \times j_{ph}) / (\lambda \times P),$$

where λ is incident wavelength and P is the intensity of incident light to the WO_3 film with consideration of transmission of the glass window and FTO glass substrate. Figure 3 shows a transmission spectrum of the FTO glass used in the present study.

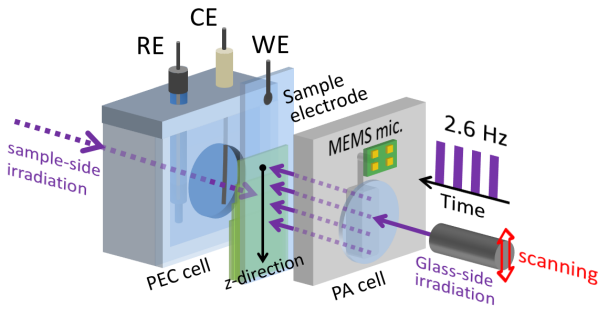

Figure 2. Schematic illustration of the system for simultaneous PEC and PA measurements.

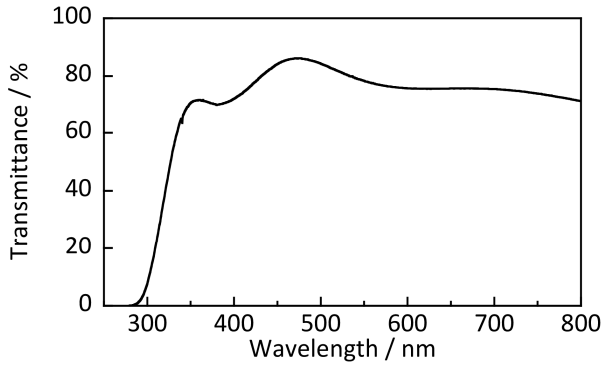

Figure 3. Transmission spectrum of the FTO glass used in the present study.

RESULTS AND DISCUSSION

PA intensity and IPCE as functions of irradiation position for a wo-PN sample

Figure S1 shows linear sweep voltammetry (LSV) curves of a wo-EC sample under photoirradiation in the thick-film region (red line) and thin-film region (blue line). Although applied potential is one of factors determining the photoelectrode performance, dependence of LSV curves on applied potential was similar, regardless of film thickness. The results indicate that the applied potential has a slight influence on optimum thickness in the present sample. Therefore, the applied potential was fixed at 960 mV vs RHE in the present study.

Figure 4 shows the PA intensity and IPCE of a wo-EC sample as functions of vertical irradiation position (glass-side irradiation). Both PA intensity and IPCE of the wo-EC sample were much larger than those of the FTO glass, indicating that PA intensity and IPCE of the wo-EC sample obtained by glass-side irradiation are attributed to photoabsorption of WO_3 deposited on the FTO glass. As shown in Figure 4a, PA intensity increased and then showed a saturation tendency as

irradiation was scanned in the z-axis direction. This is reasonable because photoabsorption increase as a film thickness and shows saturation in the case of film thickness close to penetration depth of irradiation light. The increase in WO_3 film thickness along the z-axis direction was confirmed by cross-sectional FE-SEM images (Fig. S2) while changes on the morphology were hardly observed from top-view FE-SEM images (Fig. S3). In Figure 4b, IPCE increased and then showed a saturation tendency as irradiation was scanned in the z-axis direction. The feature in Figure 4b is similar to that in Figure 4a, indicating that PEC performance depends largely on photoabsorption. About 2% of maximum IPCE value in the present study was not so high, compared to previous study. One possibility for it is because recombination rate was increased as a result of photoexcitation with high power density of focused laser beam.

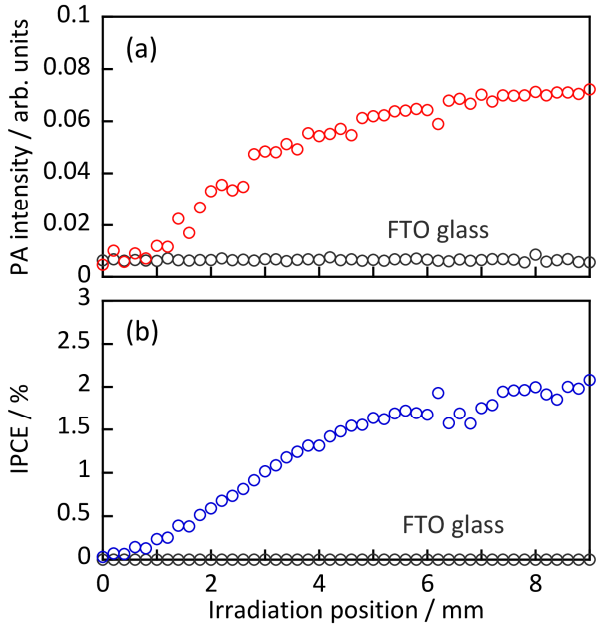

Figure 4. PA intensity and IPCE of a wo-EC sample as functions of vertical irradiation position (glass-side irradiation).

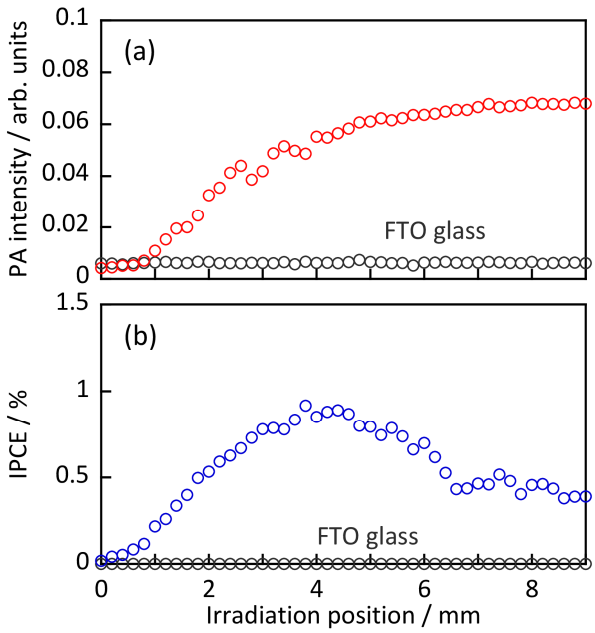

Figure 5. PA intensity and IPCE of a wo-EC sample as functions of vertical irradiation position (sample-side irradiation).

Figure 5 shows PA intensity and IPCE of a wo-EC sample as functions of vertical irradiation position (sample-side irradiation). Larger values of both PA intensity and IPCE of the wo-EC sample than those of the FTO glass were also observed, indicating that PA intensity and IPCE obtained by sample-side irradiation are attributed to photoabsorption of WO_3 deposited on the FTO glass. PA intensity measured with sample-side irradiation (Figure 5a) was similar to that measured with glass-side irradiation (Figure 4a). In contrast, a local maximum point was observed for IPCE measured with sample-side irradiation (Figure 5b). The detailed mechanism for the differences is discussed in the next section.

Correlation between photoabsorption and IPCE for a wo-PN sample

Figure 6 shows the relationship between PA intensity and IPCE. Film thickness with PA intensity of ca. 0.055 was the optimum thickness in the case of sample-side irradiation. On the other hand, results obtained by glass-side irradiation showed no local maximum point, but PA intensity of ca. 0.08, which shows saturation of photoabsorption, is presumably the optimum point. Both results obtained by glass-side irradiation and those obtained by sample-side irradiation showed almost the same linear relationship between PA intensity and IPCE in the PA intensity range of <0.04. This is reasonable since the distribution of positive holes and exited electrons in the film was almost uniform regardless of the irradiation direction when the thickness of the film is much smaller than the penetration depth. In the PA intensity range of >0.04, however, the results for glass-side irradiation and those for sample-side irradiation are clearly different. The reason for the decrease in IPCE in the case of sample-side irradiation is that most of the electrons cannot travel a long distance without recombination. On the other hand, IPCE obtained with glass-side irradiation increases as film thickness increases in all regions (Figure 4b). This is attributed to the porosity of WO_3 films, in which positive holes can react with the electrolyte that has permeated into the WO_3 film.

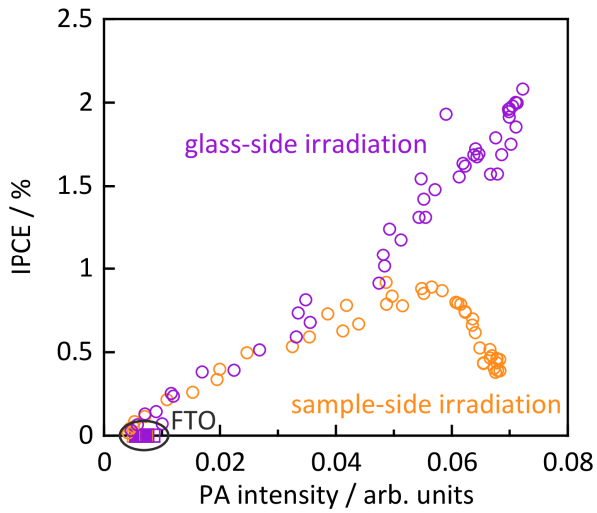

Figure 6. Relationship between PA intensity and IPCE for a wo-NP sample.

PA intensity and IPCE as functions of irradiation position for a w-PN sample

The same measurements were carried out for electrode samples with post-necking treatment. Figure 7 and 8 show PA intensity and IPCE of a w-PN sample as functions of vertical irradiation position (glass-side and sample-side irradiation, respectively). Compared to wo-PN samples, PA intensity and IPCE showed similar dependence on irradiation position regardless of the irradiation direction, but the absolute IPCE value was greatly increased. In order to discuss separately from absorption, the relationship between PA and IPCE is discussed in the following section.

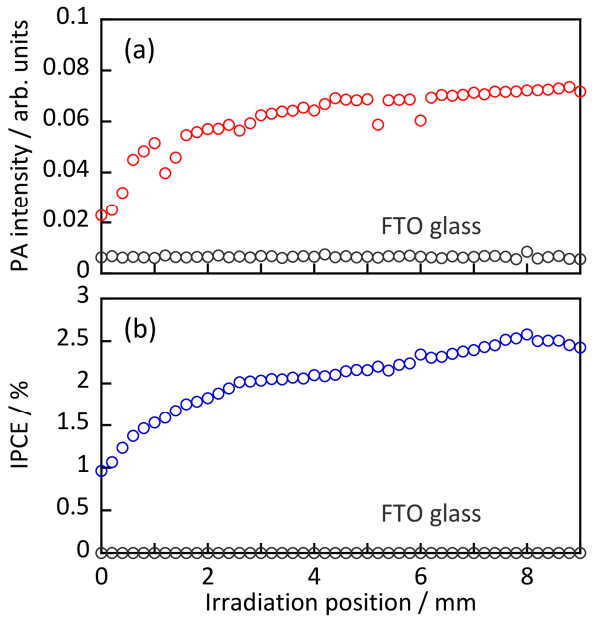

Figure 7. PA intensity and IPCE of a w-EC sample as functions of vertical irradiation position (glass-side irradiation).

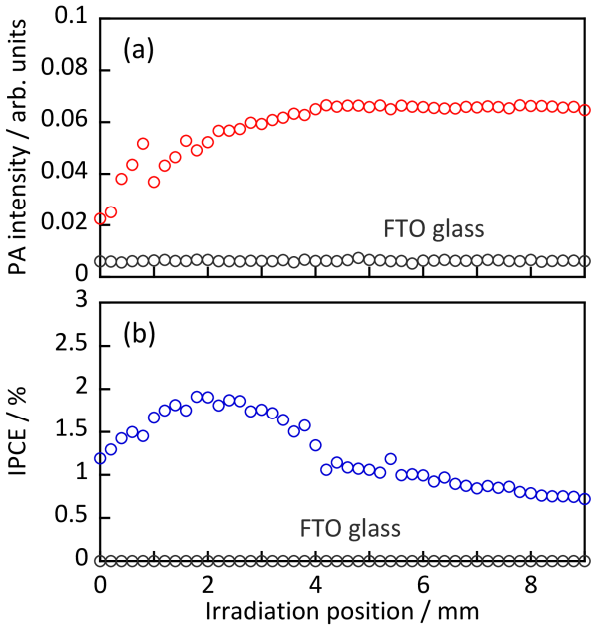

Figure 8. PA intensity and IPCE of a w-EC sample as functions of vertical irradiation position (sample-side irradiation).

Correlation between photoabsorption and IPCE for a w-PN sample

Figure 9 shows the relationship between PA intensity and IPCE. Dependence of PA intensity on IPCE for a w-PN sample was similar to that for a wo-PN sample. IPCE monotonically increased as a function of PA intensity for glass-side irradiation, while a local maximum was observed for sample-side irradiation. However, IPCE of w-PN was larger than that of wo-PN at the same PA intensity, indicating that enhancement of IPCE is not due to photoabsorption. A local maximum was observed at PA intensity of ca. 0.055 for sample-side irradiation, and this was almost the same as that in the case of glass-side irradiation. This indicate that an increase in diffusion length, which is caused by inter-particle contact and passivation of the surface state, is not the main reason for enhancement of performance by post-necking treatment. Another possibility is the formation of a WO_3 blocking layer on FTO that suppresses back electron transfer to the electrolyte solution at the FTO/electrolyte interface.[22,23]

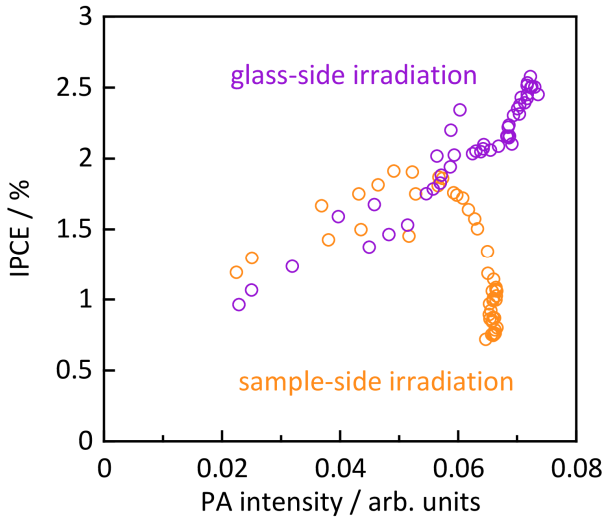

Figure 9. Relationship between PA intensity and IPCE for a w-NP sample.

CONCLUSION

In the present study, a system for simultaneous measurements of PEC reaction and photoabsorption was established using a PA technique and a photoelectrode with a film-thickness gradient. This system requires only one electrode in order to determine optimum thickness, and it is applicable to various kinds of photoelectrode (kind of semiconductor and post-treatment). This method is also useful for elucidation of the mechanism for PEC reaction from relationship between IPCE and photoabsorption.

ASSOCIATED CONTENT

Supporting Information.

The Supporting Information is available free of charge at https://pubs.acs.org/doi/10.1021/acscombsci.xxxxxxx. Cross-sectional and top-view FE-SEM images of a wo-EC sample, LSV curves of a wo-EC sample (PDF)

AUTHOR INFORMATION

Corresponding Author

Naoya Murakami − Graduate School of Life Science and Systems Engineering, Kyushu Institute of Technology, Kitakyushu 808-0196, Japan; orcid.org/0000-0003-1549-1669; Email: murakami@life.kyutech.ac.jp

Authors

Ryo Watanabe − Graduate School of Life Science and Systems Engineering, Kyushu Institute of Technology, Kitakyushu 808-0196, Japan

Complete contact information is available at: https://pubs.acs.org/10.1021/acs.iecr.XXXXXXX

Notes

The authors declare no competing financial interest.

ACKNOWLEDGMENT

This work was supported by Grant-in-Aid for Scientific Research on Innovative Areas "Innovations for Light-Energy Conversion (I^4LEC)" (Grant Number 18H05172).

REFERENCES

(1) Hisatomi, T.; Kubota, J.; Domen, K. Recent Advances in Semiconductors for Photocatalytic and Photoelectrochemical Water Splitting. *Chem. Soc. Rev.*, **2014**, *43*, 7520–7535.

(2) Sahara, G.; Kumagai, H.; Maeda, K.; Kaeffer, N.; Artero, V.; Higashi, M.; Abe, R.; Ishitani, O. Photoelectrochemical Reduction of CO_2 Coupled to Water Oxidation Using a Photocathode with a Ru(II)−Re(I) Complex Photocatalyst and a CoO_x/TaON Photoanode. *J. Am. Chem. Soc.* **2016**, *138*, 14152−14158.

(3) Windle, C.D.; Kumagai, H.; Higashi, M.; Brisse, R.; Bold, S.; Jousselme, B.; Chavarot-Kerlidou, M.; Maeda, K.; Abe, R.; Ishitani, O.; Artero, V. Earth-Abundant Molecular Z-Scheme Photoelectrochemical Cell for Overall Water-Splitting. *J. Am. Chem. Soc.* **2019**, *141*, 9593–9602.

(4) Ikeda, S.; Fujikawa, S.; Harada, T.; Nguyen, T.H.; Nakanishi, S.; Takayama, T.; Iwase, A.; Kudo, A. Photocathode Characteristics of a Spray-Deposited Cu_2ZnGeS_4 Thin Film for CO_2 Reduction in a CO_2-Saturated Aqueous Solution. *ACS Appl. Energy Mater*. **2019**, *2*, 6911–6918.

(5) Ishibashi, T.; Higashi, M.; Ikeda, S.; Amao, Y. Photoelectrochemical CO_2 Reduction to Formate with the Sacrificial Reagent Free System of Semiconductor Photocatalysts and Formate Dehydrogenase. *ChemCatChem* **2019**, *11*, 6227–6235.

(6) Lu, W.; Zhang, Y.; Zhang, J.; Xu, P. Reduction of Gas CO_2 to CO with High Selectivity by Ag Nanocube-Based Membrane Cathodes in a Photoelectrochemical System. *Ind. Eng. Chem. Res.* **2020**, *59*, 13, 5536–5545

(7) Nakajima, T.; Hagino, A.; Nakamura, T.; Tsuchiya, T.; Sayama, K. WO_3 Nanosponge Photoanodes with High Applied Bias Photon-to-Current Efficiency for Solar Hydrogen and Peroxydisulfate Production, *J. Mater. Chem. A* **2016**, *4*, 17809–17818.

(8) Hernández, S.; Saracco, G.; Barbero, G.; Alexe-Ionescu, A.L. Role of the Electrode Morphology on the Optimal Thickness of $BiVO_4$ Anodes for Photoelectrochemical Water Splitting Cells, *J. Electroanal. Chem.* **2017**, *799*, 481–486.

(9) Arai, T.; Konishi, Y.; Iwasaki, Y.; Sugihara, H.; Sayama, K. High-throughput Screening Using Porous Photoelectrode for the Development of Visible-Light-Responsive Semiconductors. *J. Comb. Chem.* **2007**, *9*, 4, 574–581.

(10) Saito, R.; Miseki, Y.; Nini, W.; Sayama, K. Discovery of Overcoating Metal Oxides on Photoelectrode for Water Splitting by Automated Screening, *ACS Comb. Sci.* **2015**, *17*, 592−599.

(11) Gutkowski, R.; Masa, J.; Schuhmann, W. A Combinatorial Approach for Optimization of Oxygen Evolution Catalyst Loading on Mo-Doped $BiVO_4$ Photoanodes, *Electroanalysis* **2019**, *31*, 1500−1506.

(12) Rosencwaig, A.; Gersho, A. Theory of the Photoacoustic Effect with Solids. *J. Appl. Phys.* **1976**, *47*, 64–69.

(13) Tam, A.C. Applications of Photoacoustic Sensing Techniques. *Rev. Mod. Phys.* **1986**, *58*, 381–431.

(14) Murakami, N.; Okuzono, K. Determination of the Internal Quantum Efficiency for Photoelectrochemical Reaction in a Semiconductor Photoelectrode by Photoacoustic Detection, *Chem. Commun.*, **2020**, *56*, 5417–5420.

(15) Shinoda, T.; Murakami, N. Photoacoustic Fourier Transform Near- and Mid-Infrared Spectroscopy for Measurement of Energy Levels of Electron Trapping Sites in Titanium(IV) Oxide Photocatalyst Powders, *J. Phys. Chem. C*, **2019**, *123*, 12169–12175.

(16) Murakami, N.; Shinoda, T. Operando Analysis of Electron Accumulation in Titanium(IV) Oxide Particles in an Aqueous Suspension Using a Photoacoustic Spectroscopic Method, *J. Phys. Chem. C*, **2019**, *123*, 222–226.

(17) Abe, R; Higashi, M.; Domen, K. Facile Fabrication of an Efficient Oxynitride TaON Photoanode for Overall Water Splitting into H_2 and O_2 under Visible Light Irradiation. *J. Am. Chem. Soc.* **2010**, *132*, 34, 11828–11829.

(18) Maeda, K.; Higashi, M.; Siritanaratkul, B.; Abe, R.; Domen, K. $SrNbO_2N$ as a Water-Splitting Photoanode with a Wide Visible-Light Absorption Band. *J. Am. Chem. Soc.* **2011**, *133*, 12334–12337.

(19) Higashi, M.; Domen, K.; Abe, R. Highly Stable Water Splitting on Oxynitride TaON Photoanode System under Visible Light Irradiation, *J. Am. Chem. Soc.* **2012**, *134*, 6968−6971.

(20) Feng, J.; Zhao, X.; Ma, S.S.K.; Wang, D.; Chen, Z.; Huang, Y. Fast and Simple Construction of Efficient Solar-Water-Splitting Electrodes with Micrometer-Sized Light-Absorbing Precursor Particles, *Adv. Mater. Technol.* **2016**, *1*, 1600119.

(21) Cao, D.; Wang, J.; Zhang, J.; Liu, S.; Xu, F.; Xu, S.; Xu, X.; Mi, B.; Gao, Z. Mechanism Investigation of the Postnecking Treatment to WO_3 Photoelectrodes. *ACS Appl. Energy Mater.* **2018**, *1*, 4670–4677.

(22) Eisenberg, D.; Ahn, H. S.; Bard, A. J. Enhanced Photoelectrochemical Water Oxidation on Bismuth Vanadate by Electrodeposition of Amorphous Titanium Dioxide. *J. Am. Chem. Soc.* **2014**, *136*, 14011–14014.

(23) Liang, Y.; Tsubota, T.; Mooij, L. P.; Van de Krol, R. Highly Improved Quantum Efficiencies for Thin Film $BiVO_4$ Photoanodes. *J. Phys. Chem. C* **2011**, *115*, 17594–17598.